MNRAS **495,** 4542–4547 (2020)
Advance Access publication 2020 May 30

doi:10.1093/mnras/staa1494

Decoupling the rotation of stars and gas – II. The link between black hole activity and simulated IFU kinematics in IllustrisTNG

Christopher Duckworth [1,2★] Tjitske K. Starkenburg,[2,3] Shy Genel,[2] Timothy A. Davis [4] Mélanie Habouzit,[5,6] Katarina Kraljic[7] and Rita Tojeiro [1]

[1] *School of Physics and Astronomy, University of St Andrews, North Haugh, St Andrews KY16 9SS, UK*
[2] *Flatiron Institute, 162 Fifth Avenue, New York, NY 10010, USA*
[3] *CIERA and Department of Physics and Astronomy, Northwestern University, 1800 Sherman Ave, Evanston, IL 60201, USA*
[4] *School of Physics & Astronomy, Cardiff University, Queens Buildings, The Parade, Cardiff CF24 3AA, UK*
[5] *Max-Planck-Institut fur Astronomie, Konigstuhl 17, D-69117 Heidelberg, Germany*
[6] *Institut für Theoretische Astrophysik, Zentrum für Astronomie der Universität Heidelberg, D-69120 Heidelberg, Germany*
[7] *Institute for Astronomy, University of Edinburgh, Royal Observatory, Blackford Hill, Edinburgh EH9 3HJ, UK*

Accepted 2020 May 20. Received 2020 May 20; in original form 2019 November 13

ABSTRACT

We study the relationship between supermassive black hole (BH) feedback, BH luminosity, and the kinematics of stars and gas for galaxies in IllustrisTNG. We use galaxies with mock MaNGA observations to identify kinematic misalignment at $z = 0$ (difference in rotation of stars and gas), for which we follow the evolutionary history of BH activity and gas properties over the last 8 Gyr. Misaligned low-mass galaxies ($M_{\rm stel} < 10^{10.2}\,{\rm M}_{\odot}$) typically have boosted BH luminosity and BH growth, and have had more energy injected by BHs into the gas over the last 8 Gyr in comparison to low-mass aligned galaxies. These properties likely lead to outflows and gas removal, in agreement with active low mass galaxies in observations. Splitting on BH luminosity at $z = 0$ produces consistent distributions of kinematic misalignment at $z = 0$; however, splitting on the maximum BH luminosity over the last 8 Gyr produces statistically significant different distributions. While instantaneous correlation at $z = 0$ is difficult due to misalignment persisting on longer time-scales, the relationship between BH activity and misalignment is clear. High-mass quenched galaxies ($M_{\rm stel} > 10^{10.2}\,{\rm M}_{\odot}$) with misalignment typically have similar BH luminosities, show lower gas fractions, and have typically lower gas phase metallicity over the last 8 Gyr in comparison to the high mass aligned.

Key words: galaxies: active – galaxies: evolution – galaxies: kinematics and dynamics.

1 INTRODUCTION

In the framework of a lambda cold dark matter Universe, galaxies form the cooling and condensation of the initial gas cloud within dark matter haloes (White & Rees 1978; Mo, Mao & White 1998). In the basic picture, they inherit the angular momentum content of the surrounding halo (Fall & Efstathiou 1980), which is obtained in the early growth phase by tidal torques from the large-scale structure (e.g. Peebles 1969; Doroshkevich 1970). As stars form the rotating gas, they inherit its dynamical characteristics often leading to coherent rotation between dark matter, gas, and stars in both magnitude and direction. However, in the non-linear regime there is good reason to believe that the rotation of dark matter, gas, and stars may decouple from each other as galaxies evolve upto $z = 0$.

Recent cosmological scale hydrodynamical simulations have provided a clear insight into the relationship between the angular momentum of baryons and dark matter through cosmic time. A necessary component of realistic simulations is efficient feedback from both supermassive black holes (BH) and stars, required to, amongst other things, reproduce late-type discs and solve the problem of catastrophic angular momentum loss (e.g. Zavala, Okamoto & Frenk 2008; Scannapieco et al. 2009). Active galactic nuclei (AGNs) and supernova explosions can also lead to dramatic redistribution of gas which regulate the angular momentum content of galaxies (e.g. Genel et al. 2015; DeFelippis et al. 2017).

'Quasar' (radiative) mode feedback releases huge amounts of energy through radiation from the accretion disc leading to high-luminosity AGNs and dramatic gas outflows (e.g. Cattaneo et al. 2009; Rubin et al. 2014; Cheung et al. 2016). Alternatively 'radio' (kinetic) mode feedback is associated with lower luminosity AGNs that host lower black hole accretion rates. In this instance, energy is deposited into the surrounding gas via jets which drive outflows,

★ E-mail: cd201@st-andrews.ac.uk

heat the gas, and suppress star formation (Binney & Tabor 1995; Ciotti & Ostriker 2001; Heckman & Best 2014).

The relationship between AGNs and kinematics has been the focus of several recent studies using integral field spectroscopy (IFS) data. In particular, a potential new class of galaxy termed 'red geyser' has been identified which host AGNs and exhibit high-velocity outflows in the spatial distribution of ionized gas (Cheung et al. 2016; Roy et al. 2018). These outflows are often linked to the existence of a distinctive offset in rotation direction between the stars and gas. Detection of ongoing outflows is, however, rare (∼5–10 per cent of the quiescent population). Penny et al. (2018) demonstrate the importance of AGN feedback in low-mass quiescent galaxies ($M_{\rm stel} < 5 \times 10^9\,{\rm M}_\odot$). While the majority demonstrate no ionized gas present, quiescent galaxies (i.e. with reduced or null SFR) with an AGN show a clear decoupling in the rotation of stars and gas. However, the relationship of gas kinematics to BH feedback is not clear for all galaxies (also see Koudmani et al. 2019). In particular, Ilha et al. (2019) find that the typical decoupling between stars and gas for AGNs defined galaxies is consistent with an inactive control sample.

Termed kinematic misalignment, the decoupled rotation of stars and gas can be a natural result of external processes (e.g. Davis et al. 2011; Barrera-Ballesteros et al. 2015; van de Voort et al. 2015; Jin et al. 2016; Bryant et al. 2019; Duckworth et al. 2019; Li et al. 2019a). Regardless of internal or external origin, kinematic misalignment in observations and simulations is linked with both a lower gas mass fraction and angular momentum (Khim et al. 2019; Starkenburg et al. 2019; Duckworth, Tojeiro & Kraljic 2020). Starkenburg et al. (2019) highlight the importance of feedback leading to gas loss, enabling new or re-accretion as a mechanism for future misalignment in low-mass galaxies. The question arises if misalignment is caused in the first instance by mergers or cosmic gas accretion (and hence making BH accretion easier) or if it is a result of AGN feedback leading to gas loss allowing for accretion of misaligned gas. The time-scales of luminous AGN are typically much shorter than kinematic misalignment, making correlation at $z = 0$ alone difficult.

In this letter, we study the temporal relationship between BH feedback, BH luminosity, and kinematic misalignment in the cosmological scale hydrodynamical simulation of IllustrisTNG100 (hereafter referred to as TNG100). We use a sample of galaxies with mock MaNGA (Mapping Galaxies at Apache Point; Bundy et al. 2015; Blanton et al. 2017) observations at $z = 0$ to emulate what we may expect to see in IFS observations. In Section 2, we briefly describe the simulation and how we construct our sample. In Section 3, we present our results before concluding in Section 4.

2 METHODS

We use the fiducial run of TNG100 which follows the evolution of a periodic cube with side lengths of 110.7 Mpc (75 h^{-1} Mpc) with mass resolution of baryonic (dark matter) elements of $1.4 \times 10^6\,{\rm M}_\odot$ ($7.5 \times 10^6\,{\rm M}_\odot$). The IllustrisTNG project (Marinacci et al. 2018; Naiman et al. 2018; Nelson et al. 2018; Springel et al. 2018; Pillepich et al. 2018a) is a suite of magnetohydrodynamic cosmological scale simulations incorporating an updated comprehensive model for galaxy formation physics (Weinberger et al. 2017; Pillepich et al. 2018b) and making use of the moving-mesh code AREPO (Springel 2010; Pakmor, Bauer & Springel 2011; Pakmor & Springel 2013). We make use of public data, as described in Nelson et al. (2019). Of particular relevance is the prescription of Weinberger et al. (2017) for BH feedback, which is modelled by two modes (quasar mode: high accretion, kinetic mode: low accretion). The transition threshold in terms of the Eddington ratio is $f_{\rm Edd} = \min(2 \times 10^{-3}(M_{\rm BH}/10^8\,{\rm M}_\odot)^2, 0.1)$ so that BHs typically transition from quasar to kinetic mode around $M_{\rm BH} = 10^8\,{\rm M}_\odot$. In the following, we separate our TNG100 galaxies by stellar mass at $M_{\rm stel} = 10^{10.2}\,{\rm M}_\odot$ (nominally referred to low- and high-mass galaxies henceforth) which corresponds to this transition (i.e. $M_{\rm BH} \approx 10^8\,{\rm M}_\odot$, see fig. 1 in Li et al. 2019b). We do not explicitly follow the individual modes of accretion and feedback for each galaxy, which can alternate through its evolutionary history. Despite this, the transition threshold in TNG determines that we almost exclusively isolate the role of radiative feedback for our low-mass sample. Our high-mass sample, however, has been subject to both quasar and kinetic feedback over the last 8 Gyr.

To emulate what we may expect to see in IFS observations we construct a sample of TNG100 galaxies with mock MaNGA observations (a complete description is given in Duckworth et al. 2020). Here, we briefly describe the sample construction. For each public MaNGA galaxy, we find a unique object in TNG100 with the closest match in stellar mass, $g - r$ colour and size. MaNGA is designed have a near flat distribution in stellar mass ($10^{8.5}\,{\rm M}_\odot < M_{\rm stel} < 10^{11.5}\,{\rm M}_\odot$). We create mock observations for each match by convolving the raw motions of all star particles/gas cells with noise and PSF typical of MaNGA. While this is sufficient for the purpose of this work, we recommend the SIMSPIN package (Harborne et al. 2019; Harborne, Power & Robotham 2020) for more in-depth mock observations. The spatial scale of the simulation is effectively set by the gravitational softening length of both the DM and stellar particles at $0.5\,h^{-1}$ kpc = 0.74 kpc. This is approximately a factor of two (four) finer than the spatial sampling (PSF full width half maximum) of a typical MaNGA observation. The typical spatial resolution of star-forming gas cells in TNG100 is of the order of ∼200 pc and therefore suitable for our mock observations. We direct the reader to fig. 1 in Pillepich et al. (2019) for further details (scale by a factor of $16^{1/3}$ for TNG100). Each galaxy is 'observed' (taking the line of sight to the be the z-axis of the box) upto the typical MaNGA footprint (1.5–2.5 effective light radii in a distinct hexagonal shape) to create mock velocity fields, from which we define the degree of misalignment between the rotation of stars and gas by fitting a position angle (PA). This is done using the `fit_kinematic_pa` routine (see appendix C of Krajnović et al. 2006) so that $\Delta{\rm PA} = |{\rm PA}_{\rm stellar} - {\rm PA}_{\rm gas}|$. We take objects with $\Delta{\rm PA} < 30^\circ$ to be aligned, $\Delta{\rm PA} \geq 30^\circ$ to be misaligned and $\Delta{\rm PA} \geq 150^\circ$ to be counter rotating. Please note that therefore the misaligned sample contains the counter-rotating sample. We have verified that removing the counter-rotating galaxies from the misaligned sample does not affect our conclusions. We only select galaxies that have distinct PAs (i.e. clear, coherent rotation) in both their stellar and gas velocity fields, leaving a total of ∼2500 galaxies used in this study. We follow the prior time evolution of BH and gas properties for each galaxy by considering the main progenitor branch (most massive defined by stellar mass) in the sublink merger trees (Rodriguez-Gomez et al. 2015). We compute BH bolometric luminosities as

$$L_{\rm bol,AGN} = \frac{\varepsilon_{\rm r}}{1-\varepsilon_{\rm r}}\dot{M}_{\rm BH}c^2, \quad (1)$$

where $\varepsilon_{\rm r} = 0.1$ is the radiative efficiency (see discussion in Habouzit et al. 2019), c the light speed, and $\dot{M}_{\rm BH}$ the accretion rate on to the BH. Gas properties are defined within two effective radii ($R_{\rm e}$, radius containing half of the stellar mass within the galaxy), unless stated otherwise.

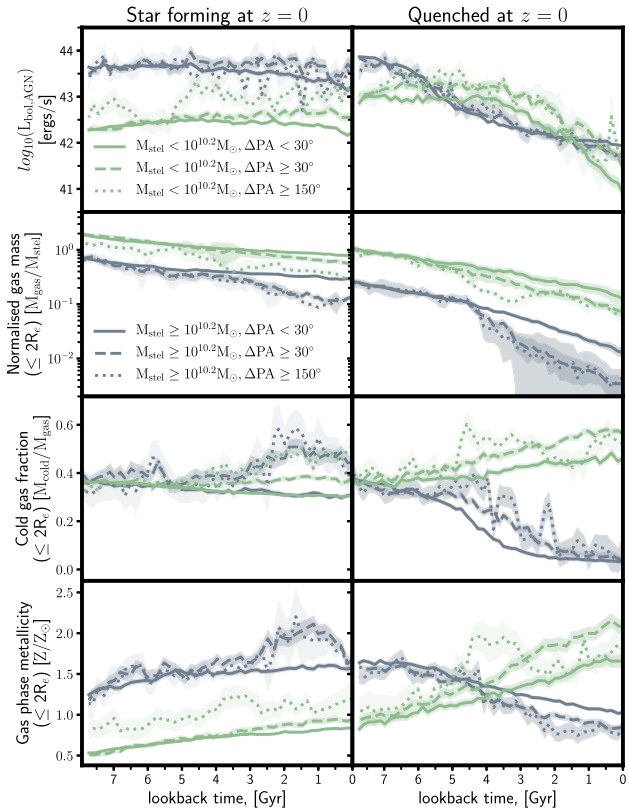

Figure 1. Time evolution of (rows top to bottom) black hole luminosity ($\log_{10}(L_{\rm bol,\,AGN})$), normalized gas mass ($M_{\rm gas}/M_{\rm stel}$), cold and star-forming gas fraction ($M_{\rm cold}/M_{\rm stel}$), and, gas phase metallicity for star-forming (left) and quenched galaxies (right) identified at $z = 0$. Galaxies are divided into low-mass (green; $M_{\rm stel} < 10^{10.2}\,{\rm M}_\odot$) and high-mass (grey; $M_{\rm stel} > 10^{10.2}\,{\rm M}_\odot$) populations. Both are subdivided by misalignment (ΔPA $<30°$: solid, $\geq 30°$: dashed, and $\geq 150°$: dotted). Each line shows the median for the population with the shaded region corresponding to the standard error.

3 RESULTS

Each panel of Fig. 1 shows the time evolution average of a property for all galaxies split by stellar mass at $M_{\rm stel} = 10^{10.2}\,{\rm M}_\odot$, as explained in Section 2. Splitting directly on BH mass at $M_{\rm BH} = 10^{8}\,{\rm M}_\odot$ or enforcing stricter stellar mass cuts does not change any of our findings. We divide our sample by ΔPA at $z = 0$. For each sub-population, we find that the stellar mass distributions are consistent at $z = 0$ for aligned and misaligned galaxies. We also split on specific star formation rate using the distance from the star-forming sequence (SFS) as defined in Pillepich et al. (2019). We select star-forming ($\Delta\log_{10}({\rm SFR}) > -0.5$) and quenched galaxies ($\Delta\log_{10}({\rm SFR}) \leq -1.0$) at $z = 0$. For clarity, the correlations with each misaligned sub-population in Fig. 1 are summarized by Table 1. Additional time evolution properties can be found in the Supplementary material, and are also summarized in Table 1. We show the population average by median; however, our results do not qualitatively change if we use the mean.

3.1 Star-forming galaxies

In Fig. 1, misaligned (dashed) and counter-rotating (dotted) low-mass star-forming galaxies (green curves in left column) exhibit increased BH luminosity (top row; $\log_{10}(L_{\rm bol,\,AGN})$) and a decreased total gas fraction within $2R_{\rm e}$ (second row; $M_{\rm gas}/M_{\rm stel}$) over the last 8 Gyr relative to those aligned (solid). In TNG, galaxies in this mass range almost exclusively exhibit quasar mode feedback, suggesting this mode's correlation with misalignment (as shown by both increased BH luminosity and potential outflows seen in a lowered gas fraction). Those misaligned also demonstrate positive correlations with the fraction of cold or star-forming gas (third row; $M_{\rm cold}/M_{\rm gas}$ where $M_{\rm cold}$ is selected by gas cells with $T < 10^{4.5}$ K or SFR > 0) and gas phase metallicity (fourth row; $Z/{\rm Z}_\odot$) compared with the aligned. It is important to note that despite the increased fraction of cold or star-forming gas for the misaligned galaxies, the overall gas mass is lower than the aligned. In particular, the higher gas metallicity for the misaligned galaxies could indicate accretion of pre-enriched or recycled material, or that fresh accretion is prevented by the radiative outflows. For each property, the misaligned population is consistent with the aligned prior to a look-back time of $\sim$5 Gyr and diverge towards $z = 0$.

High-mass star-forming galaxies (grey curves in left column) exhibit the same qualitative trends with misalignment as the low-mass star-forming galaxies, also showing positive correlations with BH luminosity, cold gas fraction, and gas phase metallicity and a negative correlation with gas fraction (see also Table 1). Despite this, these trends are notably less linear (BH luminosity aside) with bumps seen at a look-back time at $\sim$1.5 Gyr. As the total number of misaligned (counter rotating) high-mass star-forming galaxies is 31 (8) we consider the bump, while significant, too dependent on a very small set of galaxies. The similarities between the low- and high-mass star-forming galaxies could be indicative that they are subject to the same physical processes.

3.2 Quenched galaxies

Quenched low mass galaxies (green curves in right column of Fig. 1) also demonstrate positive correlations with BH luminosity, cold gas fraction and gas phase metallicity and a negative correlation with gas fraction. This appears to corroborate the possible relationship between misalignment and radiative feedback mode as seen for the star-forming low-mass galaxies. Trends of BH luminosity and gas fraction, however, are more prominent for the quenched galaxies (relative to the low mass star forming) and show deviations from the aligned galaxies at earlier look-back times. To understand this, we discuss the evolution of the black hole and related feedback in Section 3.3.

Trends for the quenched high-mass galaxies are generally less distinct. Despite this, the gas-phase metallicity is typically lower for those misaligned at $z = 0$ in contrast to the three other sub-populations. In addition, we find that despite a decreased gas fraction within $2R_{\rm e}$, the misaligned galaxies show typically higher cold gas masses (within $2R_{\rm e}$) and no overall decrease in gas mass (within the overall sub-halo) relative to the aligned (supplementary material; rows one and two). This may indicate that for the high-mass quenched galaxies the accretion of pristine gas and gas-rich minor mergers is important for decoupling their rotation. This could be a natural result of high-mass quenched galaxies hosting smaller gas reservoirs, meaning that a small amount of accretion on to the galaxy (relatively to late types) is sufficient to cause misalignment. An alternate explanation could be that enriched gas is preferentially lost due to feedback or environment.

Table 1 summarizes the correlations of galaxy properties with misalignment at $z = 0$ as discussed in this section and shown in Fig. 1, as well as those shown in the Supplementary material. Most apparent are the (strongly) positive correlations of present-day misalignment with AGN luminosity, cold gas fraction, and gas phase

Table 1. Truth table summarizing the correlations found in Fig. 1 between BH luminosity, normalized gas mass (<2R_e), cold gas fraction, and gas phase metallicity (first four columns) with misalignment identified at $z = 0$. The latter three columns additionally show the correlations found in the Supplementary material between total normalized gas mass (in sub-halo), normalized cold gas mass, and specific stellar angular momentum with misalignment. Correlations are shown individually for misaligned galaxies separated by both stellar mass and SFR at $z = 0$. ++, +(−−, −) refer to strong and mild positive (negative) correlations, 0 to no correlation and bump indicates a feature in the curve. A C is appended if the correlation/feature is only applicable to counter-rotating galaxies.

	$L_{\rm bol,\ AGN}$	$M_{\rm gas}/M_{\rm stel}$ (<2R_e)	$M_{\rm cold}/M_{\rm gas}$	$Z/Z_\odot$	$M_{\rm gas}/M_{\rm stel}$ (total)	$M_{\rm cold}/M_{\rm stel}$	$j_{\rm star}$
Low-mass star forming	++	−−	++	+	−−	0/−C	−−
High-mass star forming	+	−−	++/bump	+/bump	−−	−/bump	−−
Low-mass quenched	+	−−/bumpC	++/bumpC	++/bumpC	−−	−−	−−
High-mass quenched	0	−	+	−	0	0+	−−

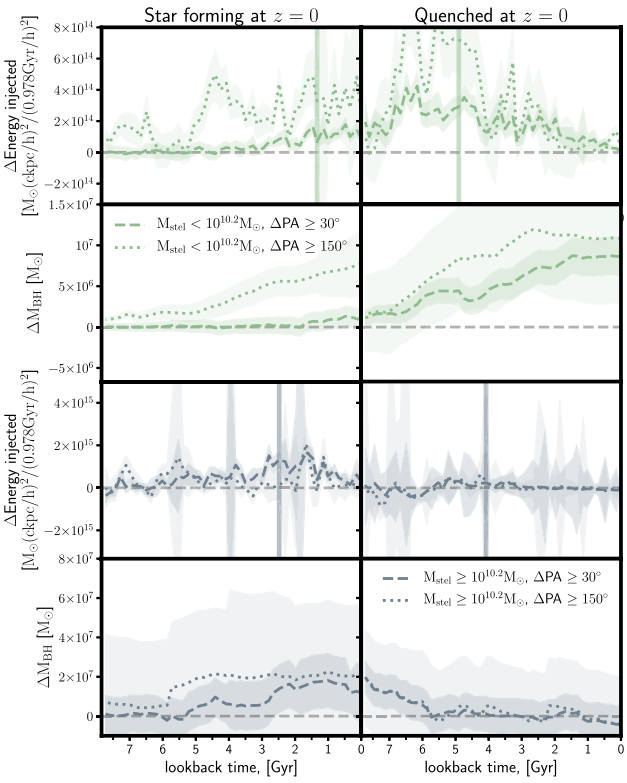

Figure 2. Time evolution of black hole feedback energy injection and black hole mass for star forming (left) and quenched galaxies (right). Each row shows the residuals (ΔEnergy injected = $E_{\rm misaligned/counter\ rotating} - E_{\rm aligned}$) or $\Delta M_{\rm BH}$ where galaxies with ΔPA ≥ 30° (dashed) and ΔPA ≥ 150° (dotted) are defined relative to ΔPA < 30°. The vertical line in the energy injection panels represents the time at which 50 per cent of the energy over the last 8 Gyr has been injected. The top (bottom) two rows show the median trends for low- (high-) mass galaxies.

metallicity, and the (strongly) negative correlations with normalized gas mass (both within 2R_e and total), and specific angular momentum. Table 1 also highlights that these correlations are less strong for the high-mass quenched galaxies, and that additional features can be found in the correlations with misalignment (bump) or only with counter rotation (bumpC) for the high-mass star-forming and the low-mass quenched galaxies, respectively.

3.3 Evolution of the black hole feedback

In Fig. 2, we show the time evolution of the mass of the black hole and of its associated feedback: the amount of energy injected into the surrounding gas cells. Here, we plot the average residual difference (ΔEnergy injected = $E_{\rm misaligned/counter\ rotating} - E_{\rm aligned}$) of misaligned (dashed) and counter-rotating (dotted) galaxies with respect to the aligned galaxies (grey-dashed line at the origin) for both the low-mass (first two rows) and high-mass galaxies (bottom two rows).

For the low-mass galaxies, we find that the rate of energy injection is typically elevated for counter-rotating galaxies; however, a clear boost can be seen for all those that are misaligned at $z = 0$. The look-back time of peak energy injection is earlier for quenched galaxies relative to the star forming (the solid vertical line represents the time at which 50 per cent of the energy over the last 8 Gyr has been injected). Misaligned star-forming galaxies show far more recent feedback and BH luminosity, possibly indicative that the feedback has not fully suppressed star formation yet. Conversely, the quenched galaxies exhibit earlier peak energy injection that through this feedback suppressing star formation leads to the quenched classification at $z = 0$. For this reason selecting misaligned star forming and quenched galaxies at $z = 0$ will naturally lead to different time correlations in BH activity.

We also show the residual time evolution of black hole mass with respect to the aligned galaxies (Fig. 2 row 2 for low-mass galaxies). We find that BH growth correlates with the time-scales of energy injection, indicating the close relationship between feedback and accretion for those misaligned. The causality between BH growth and feedback is however not clear. While BH growth leads to increased feedback by design, with respect to a possible correlation between feedback and the onset of misalignment the question of causality remains. One possibility is that the angular momentum is disrupted prior to feedback, potentially due to mergers. Alternatively, gas removal due to feedback could facilitate (re-)accretion of (misaligned) gas which disrupts angular momentum and then leads to increased BH growth. We again note that misaligned high mass star-forming galaxies (third row, left-hand panel) demonstrate the same qualitative trends with BH feedback and growth as the low mass, corroborating that radiative feedback is likely dominant for this sub-sample. Misaligned and counter-rotating high-mass quenched galaxies show little obvious trends of BH feedback energy and growth relative to the aligned.

3.4 Correlating kinematic misalignment and AGN at $z = 0$

To understand how kinematic misalignment may correlate with BH luminosity at $z = 0$ alone, in the top panel of Fig. 3, we show the distribution of ΔPA for the top 20 per cent BH luminosity in our low-mass sample ($M_{\rm stel} < 10^{10.2}\,M_\odot$, both the star forming as quenched galaxies) in comparison with a control sample (all defined at $z = 0$). The control is made by taking the closest unique

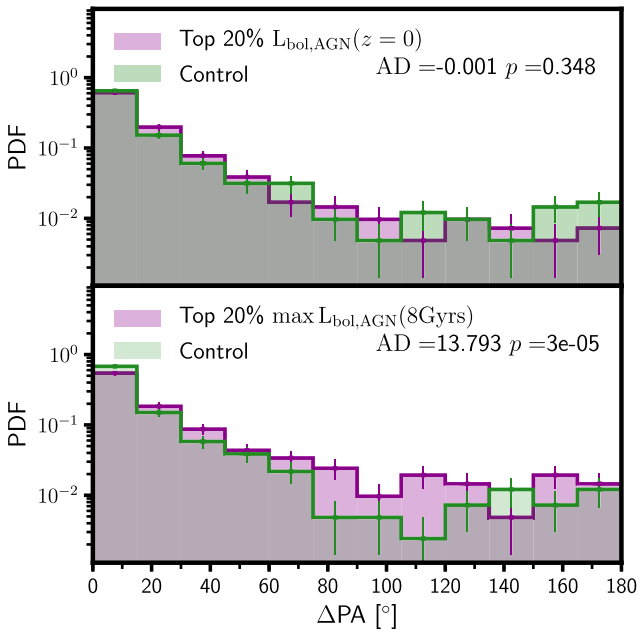

Figure 3. Probability density function of kinematic misalignment as defined by ΔPA at $z = 0$ for low-mass galaxies ($M_{stel} < 10^{10.2}$ M$_\odot$). In both panels, the brightest 20 per cent in $L_{bol,\,AGN}$ (purple) compared with a mass matched control (green) is shown. The top panel shows the brightest in $L_{bol,\,AGN}$ at $z = 0$ only, whereas the bottom panel shows those with the brightest peak $L_{bol,\,AGN}$ over the last 8 Gyr. In each panel, the Anderson–Darling statistic with a corresponding p-value is shown. We find no statistical difference between the active galaxies and the control for those selected at $z = 0$ only, whereas we find that those that have been the most luminous over the last 8 Gyr are distinctly more misaligned.

match in stellar mass for each high BH luminosity galaxy from the remainder of our sample. We find the two distributions are statistically indistinguishable (Anderson–Darling statistic; −0.001 with a p-value of 0.348). In the bottom panel, we show the same but instead we select the top 20 per cent in peak BH luminosity (for each galaxy in our low-mass sample) over the last 8 Gyr. In this instance, the AGN bright galaxies are distinctly more misaligned than the mass matched control (Anderson–Darling statistic; 13.793 with a p-value of 3×10^{-5}).

This demonstrates that despite the inherent relationship between BH luminosity, feedback, and gas kinematics, considering the overall distribution of ΔPA split on instantaneous luminosity at $z = 0$ does not necessitate that correlation is found. This matches that of observations in MaNGA (fig. 6 in Ilha et al. 2019), who also find no correlation between active galaxies and a control sample. We emphasize that while our results indicate a correlation between feedback and misalignment, the decoupled rotation of gas can remain for several Gyr after initially becoming misaligned, meaning that a single epoch is unlikely to characterize the relationship for an ensemble of galaxies.

We note that IllustrisTNG typically underproduces bright AGN ($L_{X\text{-ray}}$(2–10 keV) $> 10^{44}$ erg^{-1}) for $z \leq 1$ in contrast with observational constraints (see Habouzit et al. 2019). Given this and the uncertainty in estimating BH luminosity from simulations (treatment of radiatively efficient and inefficient AGNs and obscuration), we chose to select by percentile rather than cutting on absolute luminosity. Regardless, selecting only bright AGNs in this way or choosing a higher percentile does not change our conclusions.

4 SUMMARY

In this paper, we study the relationship between BH luminosity, BH feedback, and kinematic misalignment between stars and gas for galaxies in TNG100. We use mock observations of an IFS survey (MaNGA) built from galaxies in TNG100, to identify kinematic misalignment (ΔPA; difference in PAs of stars and gas) at $z = 0$. We split our mock IFS sample on stellar mass to separate the impact of 'quasar' feedback from 'kinetic' feedback. We follow the time evolution of BH luminosity and energy injection from BH feedback in leading up to misalignment (or counter rotation) at $z = 0$. We also compare the $z = 0$ distributions of ΔPA of the most luminous BHs in our sample against a control. Our conclusions are as follows:

(i) Low-mass galaxies ($M_{stel} < 10^{10.2}$ M$_\odot$) with misalignment (and counter rotation) at $z = 0$ typically have had boosted BH luminosity, BH growth, and significantly more energy injected into the gas over the last 8 Gyr in comparison to aligned galaxies. Gas is potentially blown out due to the AGN feedback, losing angular momentum towards $z = 0$. Along with the feedback there is an increase in the fraction of cold phase gas within $2R_e$ (seen also for all high-mass galaxies), along with an increased metallicity. These trends are seen for low-mass star-forming and quenched galaxies, and high-mass star-forming galaxies split at $z = 0$.

(ii) The epoch of peak energy injection from the quasar mode feedback is different as a function of $z = 0$ sSFR for misaligned low-mass galaxies, with higher sSFR galaxies having more recent feedback. This can be explained by the relationship between energy injection from feedback and galaxy quenching. Misaligned quenched galaxies have typically experienced peak energy injection from the BH at earlier times which has since acted to suppress star formation, whereas misaligned star-forming galaxies exhibit more recent energy injection.

(iii) Quenched high-mass galaxies ($M_{stel} > 10^{10.2}$ M$_\odot$) with misalignment (and counter rotation) at $z = 0$ typically have similar BH luminosity over the last 8 Gyr with respect to aligned galaxies and decreased gas mass is seen within $2R_e$ (but not for all gas associated with the total sub-halo). Gas phase metallicity is also lower with respect to aligned galaxies. This suggests that the origin of misalignment in massive quenched galaxies is more likely due to accretion of pristine gas or loss of enriched gas.

(iv) We find that the distributions of kinematic misalignment are statistically indistinguishable between the top 20 per cent in BH luminosity of low-mass galaxies in our sample and a mass matched control at $z = 0$. This matches observations (see fig. 6 in Ilha et al. 2019). Misalignment may initially occur at a similar time to the initial high-accretion state (and hence peak BH luminosity); however, misalignment can persist/correlate on much longer timescales. To test this we split by the top 20 per cent in maximum BH luminosity (for each galaxy) over the last 8 Gyrs in comparison with a control. We find that the most luminous AGN over the last 8 Gyrs are significantly more misaligned at $z = 0$. This result suggests that while one may not expect correlation with misalignment when considering BH activity at $z = 0$ alone, the relationship between BH luminosity and misalignment in low-mass galaxies is clear.

While this work clearly demonstrates the correlation between BH activity and kinematic misalignment, it makes no comment on causality. Further work is required to understand what triggers the initial high-accretion mode and following period of feedback for both low- and high-mass galaxies.

ACKNOWLEDGEMENTS

We thank the referee for valuable comments and suggestions that improved the paper. CD acknowledges support from the Science and Technology Funding Council (STFC) via an PhD studentship (grant number ST/N504427/1). The Flatiron Institute is supported by the Simons Foundation. We thank the IllustrisTNG team; this work was conducted using the public data release, however made use of the private data for other research. This research made use of the following packages; NUMPY (Oliphant 2006), SCIPY (Virtanen et al. 2020), MATPLOTLIB (Hunter 2007), and PANDAS (McKinney et al. 2010).

REFERENCES

Barrera-Ballesteros J. K. et al., 2015, A&A, 582, A21
Binney J., Tabor G., 1995, MNRAS, 276, 663
Blanton M. R. et al., 2017, AJ, 154, 28
Bryant J. J. et al., 2019, MNRAS, 483, 458
Bundy K. et al., 2015, ApJ, 798, 7
Cattaneo A. et al., 2009, Nature, 460, 213
Cheung E. et al., 2016, Nature, 533, 504
Ciotti L., Ostriker J. P., 2001, ApJ, 551, 131
Davis T. A. et al., 2011, MNRAS, 417, 882
DeFelippis D., Genel S., Bryan G. L., Fall S. M., 2017, ApJ, 841, 16
Doroshkevich A. G., 1970, Astrophysics, 6, 320
Duckworth C., Tojeiro R., Kraljic K., Sgró M. A., Wild V., Weijmans A.-M., Lacerna I., Drory N., 2019, MNRAS, 483, 172
Duckworth C., Tojeiro R., Kraljic K., 2020, MNRAS, 492, 1869
Fall S. M., Efstathiou G., 1980, MNRAS, 193, 189
Genel S., Fall S. M., Hernquist L., Vogelsberger M., Snyder G. F., Rodriguez-Gomez V., Sijacki D., Springel V., 2015, ApJ, 804, L40
Habouzit M. et al., 2019, MNRAS, 484, 4413
Harborne K. E., Power C., Robotham A. S. G., Cortese L., Taranu D. S., 2019, MNRAS, 483, 249
Harborne K. E., Power C., Robotham A. S. G., 2020, PASA, 37, e016
Heckman T. M., Best P. N., 2014, ARA&A, 52, 589
Hunter J. D., 2007, Comput. Sci. Eng., 9, 90
Ilha G. S. et al., 2019, MNRAS, 484, 252
Jin Y. et al., 2016, MNRAS, 463, 913
Khim D. J. et al., 2020, ApJ, 894, 106
Koudmani S., Sijacki D., Bourne M. A., Smith M. C., 2019, MNRAS, 484, 2047
Krajnović D., Cappellari M., de Zeeuw P. T., Copin Y., 2006, MNRAS, 366, 787
Li Y. et al., 2019b, preprint (arXiv:1910.00017)
Li S.-l. et al., 2019a, preprint (arXiv:1912.04522)
Marinacci F. et al., 2018, MNRAS, 480, 5113
McKinney W., et al., 2010, Proceedings of the 9th Python in Science Conference, Vol. 445. Austin, TX, p. 51
Mo H. J., Mao S., White S. D. M., 1998, MNRAS, 295, 319
Naiman J. P. et al., 2018, MNRAS, 477, 1206
Nelson D. et al., 2018, MNRAS, 475, 624
Nelson D. et al., 2019, Comput. Astrophys. Cosmol., 6, 2
Oliphant T. E., 2006, A Guide to NumPy, Vol. 1. Trelgol Publishing, USA
Pakmor R., Springel V., 2013, MNRAS, 432, 176
Pakmor R., Bauer A., Springel V., 2011, MNRAS, 418, 1392
Peebles P. J. E., 1969, ApJ, 155, 393
Penny S. J. et al., 2018, MNRAS, 476, 979
Pillepich A. et al., 2018a, MNRAS, 475, 648
Pillepich A. et al., 2018b, MNRAS, 473, 4077
Pillepich A. et al., 2019, MNRAS, 490, 3196
Rodriguez-Gomez V. et al., 2015, MNRAS, 449, 49
Roy N. et al., 2018, ApJ, 869, 117
Rubin K. H. R., Prochaska J. X., Koo D. C., Phillips A. C., Martin C. L., Winstrom L. O., 2014, ApJ, 794, 156
Scannapieco C., White S. D. M., Springel V., Tissera P. B., 2009, MNRAS, 396, 696
Springel V., 2010, MNRAS, 401, 791
Springel V. et al., 2018, MNRAS, 475, 676
Starkenburg T. K., Sales L. V., Genel S., Manzano-King C., Canalizo G., Hernquist L., 2019, ApJ, 878, 143
van de Voort F., Davis T. A., Kereš D., Quataert E., Faucher-Giguère C.-A., Hopkins P. F., 2015, MNRAS, 451, 3269
Virtanen P. et al., 2020, Nat. Methods, 17, 261
Weinberger R. et al., 2017, MNRAS, 465, 3291
White S. D. M., Rees M. J., 1978, MNRAS, 183, 341
Zavala J., Okamoto T., Frenk C. S., 2008, MNRAS, 387, 364

SUPPORTING INFORMATION

Supplementary data are available at *MNRAS* online.

Figure S1. Time evolution of (rows top to bottom) of normalized gas mass within the total sub-halo ($M_{\rm gas}/M_{\rm stel}$), normalized cold gas mass ($M_{\rm cold}/M_{\rm stel}$), and specific stellar angular momentum ($j_{\rm star}$), for star-forming (left) and quenched galaxies (right) identified at $z = 0$.

Please note: Oxford University Press is not responsible for the content or functionality of any supporting materials supplied by the authors. Any queries (other than missing material) should be directed to the corresponding author for the article.

This paper has been typeset from a TEX/LATEX file prepared by the author.